ChemPubSoc Europe

DOI: 10.1002/cphc.201601430

CHEMPHYSCHEM Articles

A Solution-Processable Liquid-Crystalline Semiconductor for Low-Temperature-Annealed Air-Stable N-Channel Field-Effect Transistors

Resul Ozdemir,[a] Donghee Choi,[b] Mehmet Ozdemir,[a] Hyekyoung Kim,[b] Sinem Tuncel Kostakoğlu,[c] Mustafa Erkartal,[a] Hyungsug Kim,[b] Choongik Kim,*[b] and Hakan Usta*[a]

A new solution-processable and air-stable liquid-crystalline n-channel organic semiconductor (2,2′-(2,8-bis(5-(2-octyldodecyl)thiophen-2-yl)indeno[1,2-b]fluorene-6,12-diylidene)dimalononitrile, **α,ω-2OD-TIFDMT**) with donor–acceptor–donor (D-A-D) π conjugation has been designed, synthesized, and fully characterized. The new semiconductor exhibits a low LUMO energy (−4.19 eV) and a narrow optical bandgap (1.35 eV). The typical pseudo-focal-conic fan-shaped texture of a hexagonal columnar liquid-crystalline (LC) phase was observed over a wide temperature range. The spin-coated semiconductor thin films show the formation of large (≈0.5–1 μm) and highly crystalline platelike grains with edge-on molecular orientations. Low-temperature-annealed (50 °C) top-contact/bottom-gate OFETs have provided good electron mobility values as high as 0.11 $cm^2(Vs)^{-1}$ and high I_{on}/I_{off} ratios of 10^7 to 10^8 with excellent ambient stability. This indicates an enhancement of two orders of magnitude (100×) when compared with the β-substituted parent semiconductor, **β-DD-TIFDMT** (2,2′-(2,8-bis(3-dodecylthiophen-2-yl)indeno[1,2-b]fluorene-6,12-diylidene)dimalononitrile). The current rational alkyl-chain engineering route offers great advantages for D-A-D π-core coplanarity in addition to maintaining good solubility in organic solvents, and leads to favorable optoelectronic/physicochemical characteristics. These remarkable findings demonstrate that **α,ω-2OD-TIFDMT** is a promising semiconductor material for the development of n-channel OFETs on flexible plastic substrates and LC-state annealing of the columnar liquid crystals can lower the electron mobility for transistor-type charge transport.

1. Introduction

The theoretical design and synthetic development of organic semiconductors with π-conjugated molecular structures have emerged in the past few decades since the first reports of organic field-effect transistors (OFETs) based on intrinsic molecular semiconductors of lutetium complexes in the late 1980s.[1,2] Small molecules offer great benefits due to their limited π-extended core, which can be readily modified with a variety of functional groups to fine-tune their optoelectronic and physicochemical properties.[3,4] In addition, the solubility, synthetic reproducibility, and final purity levels of small molecules can be superior to those of macromolecules and polymers, which is very crucial for the realization of low-cost and high-performance plastic optoelectronics.[5–9] To this end, numerous molecular semiconductors have been developed and characterized in a wide range of optoelectronic applications, such as OFETs,[10] organic photovoltaics (OPVs),[11] and organic light-emitting diodes (OLEDs)[12] and transistors (OLETs).[13] It is worth noting that, among these applications, π-conjugated small molecules have been even commercialized in active-matrix OLED displays as emissive and hole/electron transporting/blocking layers.[14] Of the molecular semiconductors studied to date, small molecules with electron-deficient π architectures and low LUMO energy levels constitute an important class of materials for air-stable electron transport in p–n junctions, bipolar transistors, and organic complementary-like circuitry (CMOS).[15–18] In addition, π-deficient small molecules can function as low-bandgap donor molecules or non-fullerene electron acceptors for use in bulk-heterojunction organic solar cells.[19,20]

In optoelectronic devices, with regard to charge-carrier injection from environmentally stable metallic electrodes, such as Au and Pt ($\varphi \approx -5.0$–-5.9 eV), inorganic oxides, such as indium tin oxide (ITO; $\varphi \approx -4.2$–-4.9 eV), or polymeric conductors, such as poly(3,4-ethylenedioxy)thiophene/poly(styrenesulfonate) (PEDOT/PSS; $\varphi \approx -5.0$ eV), the electronic energy levels of typical π-building blocks (e.g., benzene, thiophene, naph-

[a] R. Ozdemir, M. Ozdemir, M. Erkartal, Prof. H. Usta
Department of Materials Science and Nanotechnology Engineering
Abdullah Gül University
Kayseri, 38080 (Turkey)
E-mail: hakan.usta@agu.edu.tr

[b] D. Choi, H. Kim, H. Kim, Prof. C. Kim
Department of Chemical and Biomolecular Engineering
Sogang University, Mapo-gu, Seoul, 04107 (Korea)
E-mail: choongik@sogang.ac.kr

[c] Dr. S. T. Kostakoğlu
Department of Chemistry, Gebze Technical University
Gebze, Kocaeli, 41400 (Turkey)

Supporting Information and the ORCID identification number(s) for the author(s) of this article can be found under: http://dx.doi.org/10.1002/cphc.201601430.

thalene) are suitable only for hole-injection/-transport (p-channel semiconductors).[21,22] Therefore, most of the initially developed semiconductors in this field have exhibited mainly p-channel charge transport.[16] Although later studies have revealed that the majority charge-carrier sign can be inverted from p-channel to n-channel by functionalizing π cores with electron-withdrawing groups,[23] air-stable and solution-processable n-channel molecular semiconductors are still scarce. The introduction of lipophilic alkyl chains ($-C_nH_{2n+1}$) to rigid π cores has been shown to provide semiconductors with good solubility in organic solvents for convenient chemical purification/device fabrication, in addition to still promoting good molecular ordering in the thin-film phase.[24] In addition, flexible alkyl substituents attached to rigid molecular π backbones may impart thermotropic liquid-crystalline characteristics to the semiconductor molecules, which can be used to optimize their thin-film microstructure and morphology further through thermal processes.[25,26]

To this end, some of our group have previously reported a solution-processable n-channel molecular semiconductor, **β-DD-TIFDMT** (2,2′-(2,8-bis(3-dodecylthiophen-2-yl)indeno[1,2-b]fluorene-6,12-diylidene)dimalononitrile, Figure 1), based on

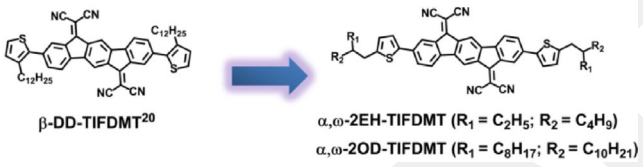

Figure 1. The chemical structures of **β-DD-TIFDMT**,[24] **α,ω-2EH-TIFDMT**, and **α,ω-2OD-TIFDMT** developed in this study.

a donor–acceptor–donor (D-A-D) π architecture with a ladder-type indenofluorenebis(dicyanovinylene) (**IFDM**) central acceptor unit and β-substituted thiophene terminal donor units. This semiconductor was found to have a low LUMO energy level of −4.32 eV, and the corresponding OFETs based on spin-coated semiconductor films showed air-stable electron mobility values (μ_e) of up to approximately 0.1 to 0.2 $cm^2(Vs)^{-1}$.[24] This π architecture was one of the early examples of non-quinoidal, air-stable n-channel semiconductors with dicyanovinylene ($C{=}C(CN)_2$) functionality, which has also guided the realization of numerous air-stable semiconductors in the past decade.[27] However, this good mobility was achieved only after annealing spin-coated semiconductor thin films at 150 to 200 °C, and the μ_e values were found to be approximately 10^{-3} $cm^2(Vs)^{-1}$ when the devices were annealed below 100 °C. For the organic semiconductor thin-film fabrication procedure to be compatible with flexible plastic substrates and underlying organic layers in multilayer devices, low-temperature ($T_{annealing} < 50$–60 °C) post-deposition annealing conditions are always more desirable. Therefore, motivated by the earlier promising semiconductor performance of this molecular π core and to realize good solution-processed μ_e values in air from low-temperature-annealed devices, we envisioned modifications to the π-core substitution from β- to α,ω-positions and the introduction of branching in the alkyl substituents. The main goals are to fine-tune the semiconductor physicochemical properties, optoelectronic characteristics, and thin-film microstructure/morphology, which can help us to understand better the effect of substitution on the charge-transport properties of this promising D-A-D π-molecular system. In addition, the current design may enhance π–π stacking interactions by minimizing the donor–acceptor dihedral angles between **IFDM** and the thiophene units, and can lead to favorable charge-transporting microstructures/morphology at low annealing temperatures ($T <$ 50–60 °C). The formation of a low LUMO energy level on a π-extended core, along with solution-processability and good electron-transport ability, will also pave the way for the new compound to be used as a non-fullerene acceptor in BHJ photovoltaic cells. To this end, we have repositioned the 3,3′-alkyl substituents to the 5,5′-positions of the terminal thiophene units, and branching was introduced at the 2-positions to give 2-ethylhexyl ($-CH_2CH(C_2H_5)C_4H_9$) and 2-octyldodecyl ($-CH_2CH(C_8H_{17})C_{10}H_{21}$) alkyl substituents. This approach is expected to benefit the extension of π conjugation along the molecular backbone and also control the π–π stacking/donor–acceptor interactions. This way, both the molecular solubility in organic solvents and the charge-transport ability in the thin film can be well maintained. To realize this delicate balance has been a conundrum in the past decade in the design of solution-processable, high-mobility n-channel semiconductors. In addition, the presence of both a rigid π unit and highly flexible, branched alkyl chains in a symmetric rod-like architecture may result in mesogenic (liquid-crystalline) behavior. Liquid-crystalline (LC) semiconductors can be quite advantageous for charge-transport in optoelectronic devices because they enable the formation of highly ordered nanostructures through molecular self-assembly. If the molecular orientation in the LC phase is matched with the charge-transport direction of a particular optoelectronic device architecture (e.g., "face-on" for OPV/OLED and "edge-on" for OFET),[28] the device performance can be further enhanced. However, because the number of high-mobility organic semiconductors that exhibit liquid-crystalline behavior has been limited in OFETs,[29] the realization of new thermotropic LC semiconductors is very valuable to tune the thin-film microstructure/morphology by post-deposition thermal annealing processes. This can be used to study and elucidate the crucial relationships between chemical structure, thin-film microstructure/morphology, and charge transport.[30]

Herein, we report the design, synthesis, and characterization of two new highly electron-deficient D-A-D-type small molecules **α,ω-2EH-TIFDMT** (2,2′-(2,8-bis(5-(2-ethylhexyl)thiophen-2-yl)indeno[1,2-b]fluorene-6,12-diylidene)dimalononitrile) and **α,ω-2OD-TIFDMT** (2,2′-(2,8-bis(5-(2-octyldodecyl)thiophen-2-yl)indeno[1,2-b]fluorene-6,12-diylidene)dimalononitrile; Figure 1). Whereas 2-ethylhexyl substitution was found to be inefficient for required solubility, substitution with 2-octyldodecyl rendered **α,ω-2OD-TIFDMT** freely soluble in various solvents, such as chloroform, THF, and toluene, at room temperature. The chemical characterizations were performed by using $^1H/^{13}C$ NMR spectroscopy, MALDI-TOF spectrometry, elemental analysis, and attenuated total reflection infrared spectroscopy

(ATR-FTIR) to elucidate the chemical structures and final purity levels. Differential scanning calorimetry (DSC) and thermogravimetric analysis (TGA) (T_{onset} = 380 °C) were performed along with melting-point analysis ($T_{c.p.}$ = 230–231 °C) to characterize the thermal properties of the new semiconductor. Compound **α,ω-2OD-TIFDMT** was found to exhibit liquid-crystalline behavior over a broad temperature range (ΔT = 90–130 °C) with the characteristic fan-shaped texture of a hexagonal columnar phase. UV/Vis absorption and cyclic voltammetry characterizations showed that **α,ω-2OD-TIFDMT** has low HOMO and LUMO energy levels of −5.64 and −4.19 eV, respectively, with a narrow solid-state optical bandgap (1.35 eV). The high solubility of **α,ω-2OD-TIFDMT**, endowed by branched α,ω-alkyl substituents, allowed the fabrication of bottom-gate/top-contact OFET devices by spin-coating. The devices, which were annealed only at 50 °C, exhibited perfectly air-stable n-channel behavior with good electron mobility values of up to 0.11 $cm^2(Vs)^{-1}$ and I_{on}/I_{off} ratios of 10^7 to 10^8. This indicates an enhancement of two orders of magnitude (100×) in charge transport, as compared with OFETs based on the low-temperature-annealed parent semiconductor (**β-DD-TIFDMT**) thin-films, which reflects the result of rational alkyl-chain engineering. Atomic-force microscopy (AFM) and out-of-plane θ–2θ X-ray diffraction (XRD) characterizations of these thin films indicate the formation of highly interconnected, micron-sized (≈0.5–1.0 μm) platelike grains with high crystallinity and edge-on molecular orientations. A decrease of four orders of magnitude (10000×) in electron mobility was observed when the semiconductor thin films were annealed in the LC state.

2. Results and Discussion

2.1. Synthesis and Structural/Thermal Characterizations

The synthetic routes to **α,ω-2EH-TIFDMT** and **α,ω-2OD-TIFDMT** are shown in Scheme 1, and involve Stille cross-coupling protocols followed by Knoevenagel condensations. The synthesis of the key indeno[1,2-b]fluorene-6,12-dione π core, **IFDK-Br2**, was previously reported by our group and the details can be found in the Supporting Information.[6] In the cross-coupling reaction, **IFDK-Br2** was reacted with the corresponding trimethyltin-substituted thiophene reagent in the presence of a $Pd(PPh_3)_2Cl_2$ catalyst to give thiopheneindeno[1,2-b]fluorene-6,12-dionethiophene compounds **1** and **2** in 48 and 34% yields, respectively. For this reaction, the best conditions were determined to be highly polar dimethylformamide (DMF) as the solvent at 125 °C, which partially dissolved the **IFDK-Br2** π core at high temperature for the cross-coupling reaction. Conversion of carbonyl (C=O) groups to dicyanovinylene ($C=C(CN)_2$) on the indeno[1,2-b]fluorene π cores of **1** and **2** was achieved by a double Knoevenagel condensation reaction with excess malononitrile in the presence of $TiCl_4$ Lewis acid and pyridine base. In this reaction, different from typical Knoevenagel condensations, the desired product formation was not observed in the absence of $TiCl_4$ Lewis acid. This indicates that $TiCl_4$ is crucial to the formation of the highly electron-deficient indenofluorenebis(dicyanovinylene) (**IFDM**) π core, and it probably plays a key role in the dehydration step. Whereas **α,ω-2EH-TIFDMT** was found to be an insoluble compound, **α,ω-2OD-TIFDMT** was freely soluble in common nonprotic organic solvents, such as chloroform, THF, and toluene, which allowed convenient chromatographic purification and thin-film solution processing (see below). This clearly reveals the effect of the different lengths of the alkyl substituents (2-octyldodecyl vs. 2-ethylhexyl) on the current D-A-D π structure. Therefore, only **α,ω-2OD-TIFDMT** was isolated in its pure form as a dark-colored microcrystalline solid in 72% yield.

Chemical structures and purities for all the intermediate and final compounds were characterized by using ^1H and ^{13}C NMR spectroscopy (Figures S1 and S2 in the Supporting Information), MALDI-TOF (Figure S3), elemental analysis, and ATR-FTIR (Figure S4). The ^1H NMR chemical shifts of non-exchangeable aromatic protons for **α,ω-2OD-TIFDMT** were highly dependent on the concentration. As shown in Figure 2, an increase in the concentration of **α,ω-2OD-TIFDMT** (from 1–16 mg mL^{-1}) in $CDCl_3$ leads to high-field shifts ($\Delta\delta_{a-f}$ = 0.1–0.3 ppm) in the ^1H NMR spectrum, which arises from the shielding effect (ring current effect) of the aromatic units between **α,ω-2OD-TIFDMT** molecules. This indicates the presence of strong self-association between **α,ω-2OD-TIFDMT** molecules in the solution phase. It is worth noting that, based on the chemical shifts measured for the current concentration changes (0.9→3.6→14.4 mM), the self-association between **α,ω-2OD-TIFDMT** molecules is expected to be as strong as that measured for previously reported macrocyclic π-conjugated systems, if not stronger.[31] This is probably a result of highly favorable inter-

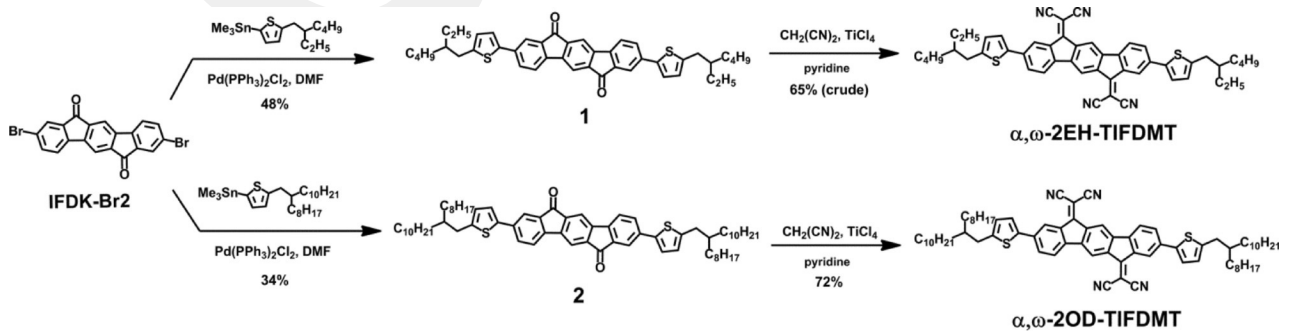

Scheme 1. Synthesis of **α,ω-2EH-TIFDMT** and **α,ω-2OD-TIFDMT**.

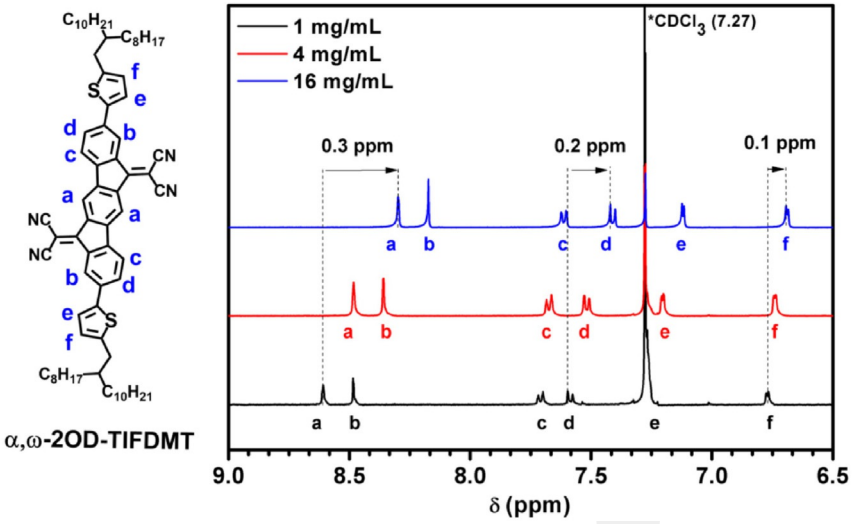

Figure 2. The concentration-dependent ^{1}H NMR spectra of **α,ω-2OD-TIFDMT** in $CDCl_3$, showing the chemical shifts of aromatic protons a–f.

molecular interactions, such as donor–acceptor, dipole–dipole, and π–π stacking between D-A-D π cores.

As shown in Figure S4, the ATR-FTIR spectrum of **α,ω-2OD-TIFDMT** shows only a C≡N (2223 cm^{-1}) stretching vibrational peak with no C=O (1700 cm^{-1}) peak, which indicates complete conversion of carbonyl groups to dicyanovinylene. The thermogravimetric analysis (TGA) of **α,ω-2OD-TIFDMT** shows the excellent thermal stability of this compound, with the thermolysis onset temperature (5% weight loss in TGA, Figure 3A) located at 380 °C. As shown in Figure 3B, the differential scanning calorimetry (DSC) measurement of **α,ω-2OD-TIFDMT** shows several sharp endothermic peaks at 85 (ΔH = 19.03 J g^{-1}), 117 (ΔH = 13.74 J g^{-1}), and 139 °C (ΔH = 10.06 J g^{-1}) prior to the isotropic transition at 232 °C (ΔH = 6.12 J g^{-1}). This isotropic transition temperature correlates perfectly with the temperature (230–231 °C) measured in the conventional melting-point analysis. In addition, the observed clearing temperature is in the same range as that of the β-substituted parent compound, **β-DD-TIFDMT** (m.p. 232–233 °C),[32] which indicates that two opposing structural effects are mostly balanced between the two semiconductors: the steric bulk of the flexible alkyl substituents (2-octyldodecyl > *n*-dodecyl) and the π rigidity/co-planarity of the molecular backbone (Figure S5; dihedral angle (θ_{Ph-Th}) = 22 (**α,ω-2OD-TIFDMT**) vs. 48° (**β-DD-TIFDMT**)). Upon cooling, two exothermic peaks at 225 (ΔH = −5.29 J g^{-1}) and 86 °C (ΔH = −12.54 J g^{-1}) were recorded. These observed DSC characteristics are indicative of a typical liquid-crystalline (LC) material,[33,34] and the **α,ω-2OD-TIFDMT** powder was further examined by using a polarized optical microscope (POM) to observe the formation of mesomorphic features as a function of temperature. The typical pseudo focal-conic fan-shaped texture of a hexagonal columnar (Col_h) liquid crystal phase was observed in the second heating cycle when the temperature was raised above 139 °C (Figure 3d).[35] Therefore, the endothermic peak at 139 °C with an enthalpy of 10.06 J g^{-1} was assigned to a crystal-to-mesophase transition. The XRD pattern (Figure S6A) of **α,ω-2OD-TIFDMT** in the LC state further confirmed the Col_h phase by showing distinct diffraction peaks ((100), (110), (200), and (210)) that correspond to lattice parameter of a = 25.81 Å.[36,37] Considering that the total length of the **T-IFDM-T** π core (18.9 Å, Figure S5), calculated from the energy-minimized molecular geometry and the alkyl-chain dimensions (4.33 Å) from the powder XRD pattern, corresponds to d_{100} in the LC phase, we propose a possible model for the molecular organization within the columns of **α,ω-2OD-TIFDMT**, which includes the formation of molecular discs by coupling molecular dimers through strong intermolecular interactions (Figure S6B).[35] In addition, an intra-columnar distance of 3.52 Å was measured from the XRD spectra, which corresponds to π–π stacking distances between molecular discs. This indicates the formation of a favorable charge-transport network along the column for optoelectronic devices. Conversely, the earlier DSC peaks at 85 and 117 °C did not result in formation of any LC phase (Figure 3a–c); therefore, they are attributed to crystal-to-crystal transitions.[25] The mesophase (Figure 3d,e) was found to be stable over a wide temperature range of approximately 90 °C until the mesophase-to-isotropic liquid transition (Figure 3f), which occurs at 232 °C. In the cooling cycle, the mesophase again remained stable over a broad temperature range from 225 to 86 °C, which can be attributed to the presence of a high degree of molecular ordering as a result of favorable intermolecular interactions (see above). During cooling of the LC phase, another important feature of the current semiconductor was observed, that is, both edge-on (homogeneous) and face-on (homeotropic) molecular alignments existed on the hydrophilic glass substrate.[28] This was clearly evident in the optical images of the same substrate during cooling (Figure S7). The presence of peripheral swallow-tailed alkyl substituents (2-octyldodecyl) on the thiophene donor units, which are attached directly to the highly π-rigid **IFDM** acceptor core, makes the current molecular design favorable for columnar liquid crystals. Similar columnar phases have been observed in the literature with alkyl-substituted rod-like π-conjugated molecular systems.[29,35,38]

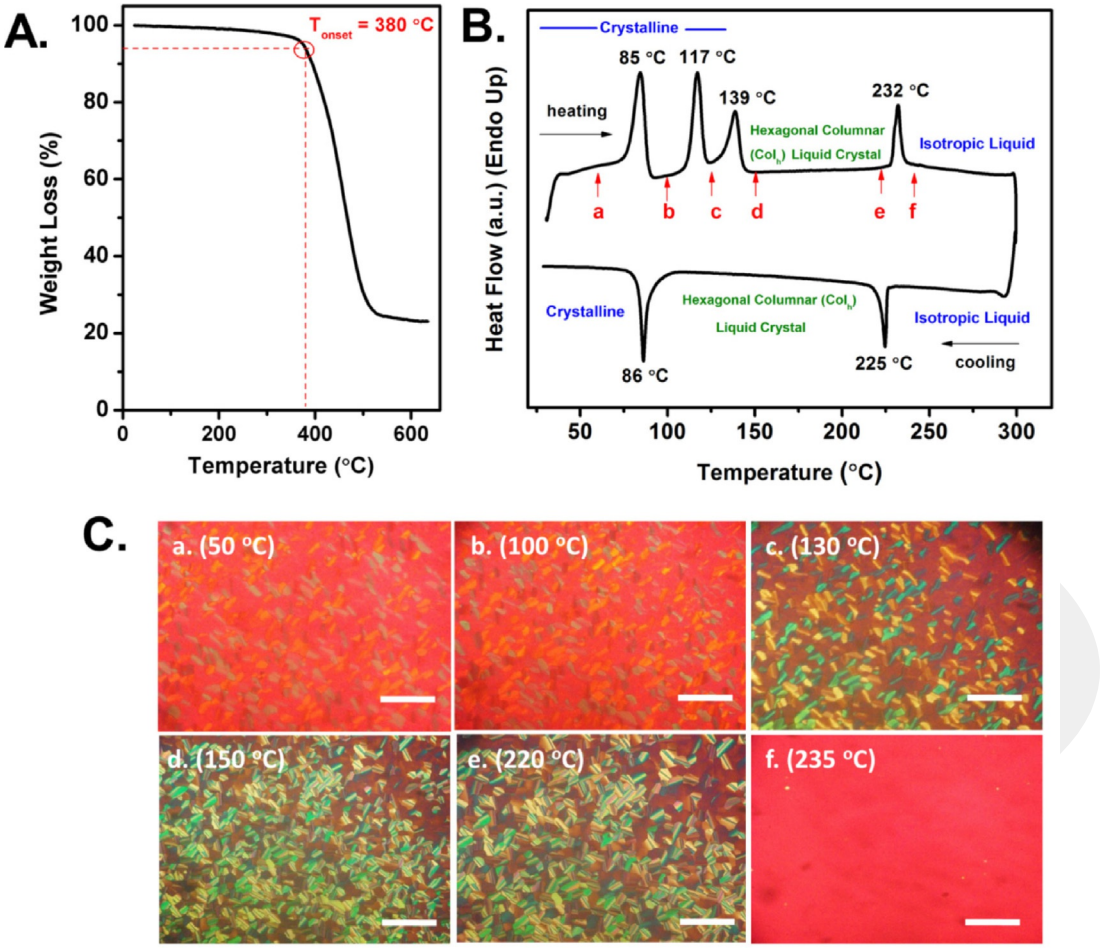

Figure 3. A) Thermogravimetric analysis (TGA) and B) differential scanning calorimetry (DSC) of **α,ω-2OD-TIFDMT** at a temperature ramp of 10 °C min^{-1} under N_2. C) Optical images taken under 90° cross-polarization conditions as a function of temperature (a–f); scale bars are ≈100 μm.

2.2. Optoelectronic Characterizations and Computational Modeling

The molecular electronic structure of **α,ω-2OD-TIFDMT** was evaluated by using UV/Vis absorption spectroscopy, cyclic voltammetry, and computational modeling (DFT, B3LYP/6-31G**). As shown in Figure 4A, two main absorption peaks at $\lambda = 353$ and 721 nm were observed for a solution of **α,ω-2OD-TIFDMT** in dichloromethane, and correspond to a π–π* transition of the indeno[1,2-b]fluorene-thiophene backbone and a symmetry-forbidden *n*–π* transition of dicyanovinylene groups, respectively.[39] When **α,ω-2OD-TIFDMT** was spin-coated as a thin film on a glass substrate, the absorption maxima were shifted to longer wavelengths by $\lambda = 36$ to 103 nm and vibronic features with peak intervals of 0.15 to 0.20 eV (aromatic C=C bond stretches) appeared. This may reflect molecular π-backbone planarization and intermolecular interactions in the thin-film state as compared with the solution phase. In addition, the optical bandgap estimated from the low-energy band edge was lowered from 1.45 (in solution) to 1.35 eV (solid state). The thin-film absorption spectra of **α,ω-2OD-TIFDMT** was found to span a wide spectral range of $\lambda = 300$ to 900 nm, which is consistent with its dark color in the solid state. Note that this also offers potential for use in photovoltaic applications as a means of harvesting a wide range of the solar spectrum. Electrochemical characterization revealed four reversible reduction peaks (Figure 4B) with the first half-wave potential located at −0.21 V (vs. Ag/AgCl), which indicates that **α,ω-2OD-TIFDMT** has very stable n-doping/dedoping characteristics with a potential electron-transporting nature.

The HOMO and LUMO energy levels were estimated as −5.64 and −4.19 eV, respectively, which are both higher than those of the reference compound, **β-DD-TIFDMT**.[32] This follows the same trends as the theoretical values (DFT, B3LYP/6-31G**) and is attributed to the repositioning of β-substitution to the α,ω-positions, which enhances the co-planarity of the D-A-D π core (Figure S5; dihedral angle (θ_{Ph-Th}) = 48→22°) and increases the HOMO ($\Delta E = 0.23$ eV) and LUMO ($\Delta E = 0.12$ eV) energies, with a larger magnitude in the former (Figure 4C). Because the HOMO is delocalized over the whole aromatic framework, as opposed to the LUMO, which is localized on the π-acceptor part, co-planarization electronically affects the HOMO more than the LUMO. The low LUMO energy level of the current semiconductor is in the same range as those of previously reported air-stable n-channel semiconductors.[16,40] Furthermore, a finely tuned LUMO energy level (increased) and optical

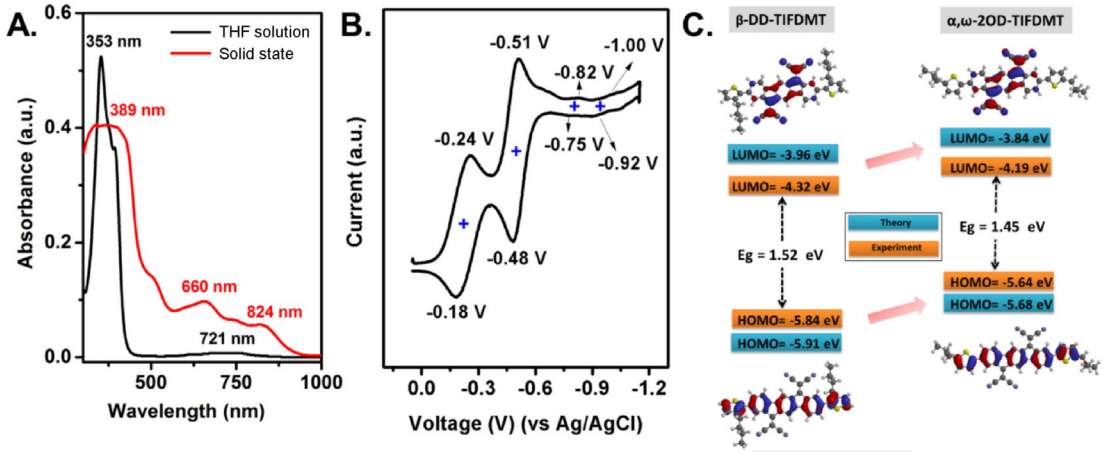

Figure 4. A) Optical absorption of **α,ω-2OD-TIFDMT** in solution in dichloromethane and as thin films, B) cyclic voltammogram of **α,ω-2OD-TIFDMT** in dichloromethane (0.1 M $Bu_4N^+PF_6^-$, scan rate = 50 mV s^{-1}), and C) calculated (in blue; DFT, B3LYP/6-31G**) and experimental (in orange) HOMO and LUMO energy levels with topographical orbital representations of **β-DD-TIFDMT**[32] and **α,ω-2OD-TIFDMT**.

bandgap (reduced) of **α,ω-2OD-TIFDMT**, as compared with **β-DD-TIFDMT**, can be advantageous for high open-circuit voltage and enhanced solar spectrum absorption when used in bulk-heterojunction solar cells as a non-fullerene acceptor.[41]

2.3. Field-Effect Transistor Fabrication and Characterization

Based on the good solubility and favorable molecular energetics, field-effect transistors (OFETs) with a top-contact/bottom-gate (TC/BG) device configuration were fabricated by spin-coating a semiconductor layer (40–50 nm) under ambient conditions. The spin-coating process was performed by using the semiconductor formulation in a high-boiling-point solvent (8 mg mL^{-1} in 1,2,4-trichlorobenzene, b.p. = 214 °C) and spinning at a slow spin rate (300 rpm for 900 s) to form large crystallites.[42] The semiconductor thin films were thermally annealed at different temperatures (50, 100, and 150 °C) for 30 min before deposition of the top source-drain gold electrodes; this annealing was found to have substantial effects on the corresponding OFET performances. Because the semiconductor layer is in direct contact with air in this device, it provides valuable information about the intrinsic air stability of the semiconductor layer during device operation without the help of any encapsulation. Highly n-doped Si with a 300 nm thermally grown SiO_2 dielectric layer was used as the gate–dielectric platform, and the dielectric surface was functionalized with a PS (polystyrene) brush to reduce surface energy and to induce a favorable semiconductor morphology/microstructure at the semiconductor–dielectric interface.[43] All transistors exhibited typical n-channel field-effect characteristics under ambient conditions. Representative transfer/output curves are shown in Figure 5. For the devices annealed at 50 °C, an average electron mobility of 0.07 to 0.11 $cm^2(V\,s)^{-1}$, an I_{on}/I_{off} ratio of 10^7 to 10^8, and a threshold voltage of approximately 19 V

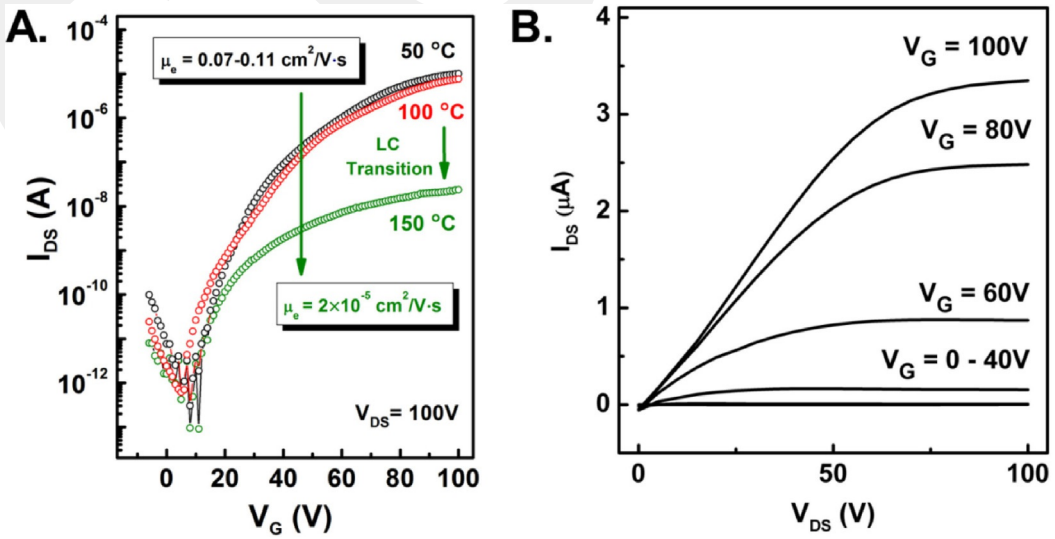

Figure 5. A) Transfer curves of the TC/BG OFETs of solution-processed thin films of **α,ω-2OD-TIFDMT** annealed at 50, 100, and 150 °C. B) Output curve of the OFET devices annealed at 50 °C.

were achieved based on 10 individual devices. This indicated a significant improvement in the charge-transport performance of the new semiconductor, with an enhancement of two orders of magnitude (100×) in electron mobility compared with TC/BG OFETs based on low-temperature-annealed ($T<$ 100 °C) **β-DD-TIFDMT** films.[32] The devices were found to be perfectly stable in air, which reflects the sufficiently low LUMO energy level of **α,ω-2OD-TIFDMT** that stabilizes charge-transporting electrons against the ambient redox couple (O_2/H_2O).[44] Devices stored under ambient conditions in the light showed only a very small degree of degradation in transfer characteristics, with a decrease of less than one order of magnitude in the on current (I_{on}) after 8 weeks of storage (Figure S8). The excellent stability of the off current ($I_{off} \approx 10^{-13}$–10^{-12} A) indicated negligible chemical doping of the semiconductor film under ambient conditions. This observed ambient stability for **α,ω-2OD-TIFDMT** is very similar to that of the OFET devices fabricated with **β-DD-TIFDMT** films, and it can be ascribed to the perfectly balanced LUMO energy level (−4.19 eV) of **α,ω-2OD-TIFDMT**, which is low enough to induce ambient stability for electron transport, but at the same time high enough to avoid any undesired chemical doping.[45] The good electron mobility and ambient stability of the current semiconductor thin films offer important advantages for **α,ω-2OD-TIFDMT** to be used in p–n junctions, bipolar transistors, and organic complementary-like circuitry (CMOS).[16] As shown in Figure 5A, when the devices were annealed at 100 and 150 °C, lower electron mobility values of 0.04 to 0.06 (I_{on}/$I_{off} = 10^7$–10^8) and 2×10^{-5} $cm^2(Vs)^{-1}$ ($I_{on}/I_{off} = 10^4$–10^5) were obtained, respectively. This is in sharp contrast to OFETs fabricated with the parent semiconductor, **β-DD-TIFDMT**, in which thermal annealing of the film gradually increased μ_e from $\approx10^{-3}$ to 0.16 $cm^2(Vs)^{-1}$ as a result of microstructural rearrangements and increases in grain size.[32] The observed mobility trend for the new LC semiconductor's OFET performance correlates with microstructural and morphological changes in the thin-film phase, as discussed below.

2.4. Thin-Film Microstructure and Morphology

Morphological and microstructural characterizations of the semiconductor thin films were carried out by using atomic force microscopy (AFM) and out-of-plane θ–2θ X-ray diffraction (XRD) techniques. As shown in Figure 6A, thin films annealed at 50 °C formed highly interconnected, micrometer-sized (≈0.5–1.0 μm) platelike grains of terraced islands with step heights of approximately 3.9 nm (Figure 7A). This correlates well with the *d*-spacing (3.79 nm) measured along the lamellar layers based on the out-of-plane XRD scan. For films annealed at 100 °C, the morphology changed to larger grains (>1.0–2.0 μm) with sharp edges and loose interconnectivity (Figure 6B). The step-height profile (Figure 7B) obtained from the AFM image indicates the formation of cracks as deep as around 25 to 40 nm between the crystalline grains, which almost reached the surface of the underlying substrate. This temperature is right above the first endothermic transition (85 °C) observed in the DSC scan, and it probably results in molecular rearrangements in the crystalline grains to give larger grains at the cost of deteriorated interconnectivity. This is also obvious in the XRD scan (Figure 6B), in which some additional diffraction peaks appeared at the higher-angle region (7–15°) that probably belong to a secondary crystalline phase. Finally, when the films were annealed at 150 °C in the LC state, the film morphology completely changed to continuous two-dimensional lamellar layers with step-heights of approximately 3.9 nm (Figure 7C) that uniformly covered the 10×10 μm^2 scan area.

θ–2θ X-ray diffraction (XRD) characterizations of the thin films revealed the formation of a highly crystalline texture with a single set of Bragg diffraction peaks up to the eleventh order (00 11). This is indicative of long-range molecular ordering throughout the film thickness in the out-of-plane direction. Based on the first (001) diffractions observed at $2\theta = 2.34°$ (for 50 °C annealing), $2\theta = 2.42°$ (for 100 °C annealing) and $2\theta = 2.28°$ (for 150 °C annealing), lamellar *d*-spacings of 37.9, 36.6, and 38.7 Å were measured in the out-of-plane direction, respectively. When these *d*-spacings were compared with the computed molecular length (energy-minimized geometry calculated by using DFT, B3LYP/6-31G**; Figure S5B, 40.9 Å) for the fully extended alkyl substituents, it is very likely that, in all thin films regardless of the annealing temperature, the molecules mostly adopt an edge-on orientation with a small degree of alkyl-chain interdigitation and/or molecular tilting from the substrate normal. For thin films annealed at 50 and 100 °C, Laue oscillations were observed around the first-order (001) diffraction peaks, which indicated that the crystallite spacings were perfectly uniform throughout the thickness of the semiconductor layer.[46] The observed favorable microstructure and morphology of the semiconductor thin film annealed at 50 °C is a result of strong intermolecular interactions between the properly designed molecular structures of **α,ω-2OD-TIFDMT** and clearly explains the observed good electron mobility under ambient conditions after a relatively low annealing temperature. This clearly explains the increase in mobility by two orders of magnitude (100×) compared with **β-DD-TIFDMT**. Note that the observed densely packed film morphology should benefit the formation of a physical barrier against the diffusion of ambient redox species (O_2 and H_2O) and contribute to the ambient stability of devices based on the current semiconductor thin films. Although the crystalline grains became larger and the molecular edge-on orientation was maintained when the thin films were annealed at 100 °C, the observed twofold decrease in electron mobility should originate from the deterioration in the connectivity of these grains. Finally, it is very surprising that, despite the favorable lamellar morphology and the crystalline microstructure (with edge-on molecular orientation), an extremely low electron mobility value of 2×10^{-5} $cm^2(Vs)^{-1}$ was observed when the semiconductor thin films were annealed at 150 °C. This is in contrast to the mainstream observations for semiconductor thin films: that surface morphology and bulk crystallinity typically explains the OFET performance well. Therefore, it is very likely that **α,ω-2OD-TIFDMT** molecules adopt a somewhat different and unfavorable microstructure/morphology in the bottom few layers at the

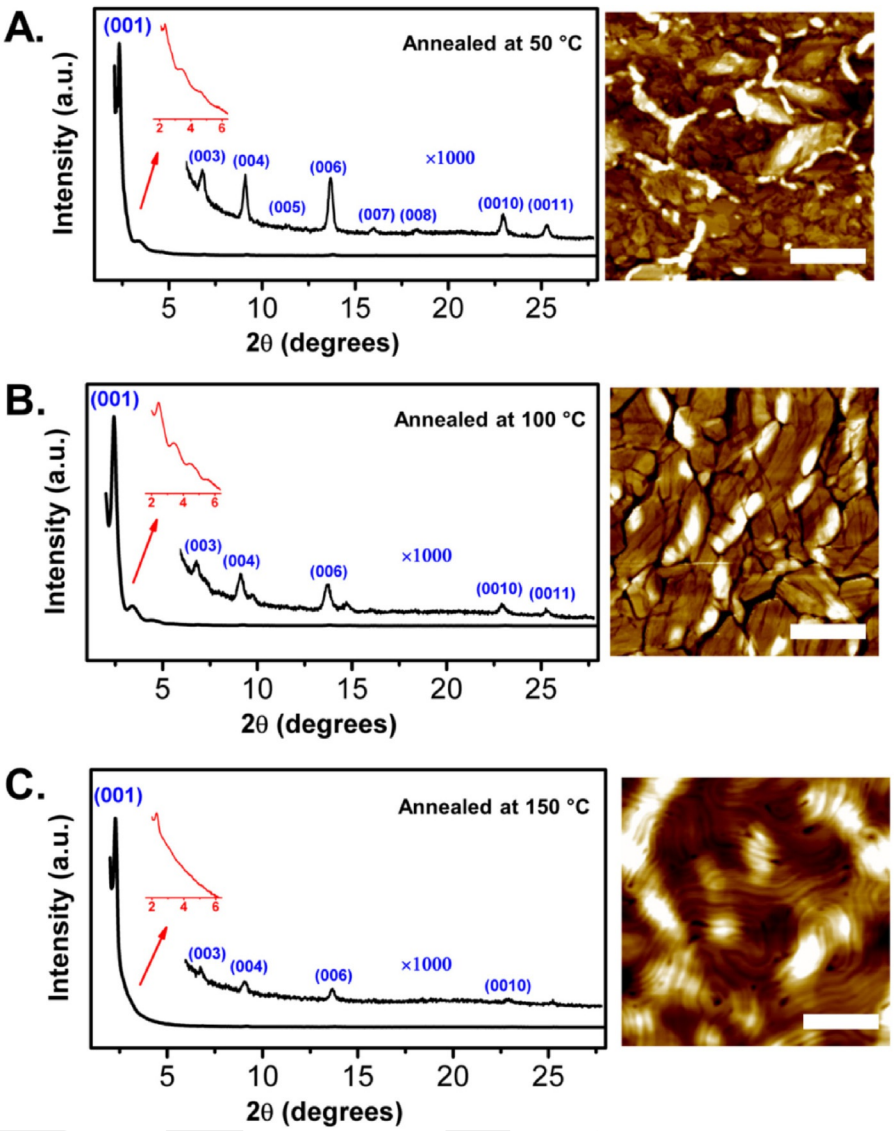

Figure 6. θ–2θ out-of-plane X-ray diffraction (XRD) scans and AFM topographic images of spin-coated **α,ω-2OD-TIFDMT** thin films annealed at a) 50, B) 100, and C) 150 °C; scale bars are 2.5 μm. Insets: Close-ups of the Laue oscillations around the (001) diffraction peak.

semiconductor–dielectric interface, compared with those of the bulk thin film. Although the exact nature of the semiconductor's microstructure/morphology at this interface requires further advanced analysis, it should be related to a molecular orientation remnant from the LC phase. Note that, for semiconductor thin films, the charge-transport process occurs mostly through the first few molecular layers at the dielectric–semiconductor interface.[47] Given the significant drop in charge transport, although the majority of the semiconductor thin film shows a highly ordered edge-on orientation, we speculate that molecules at the interface probably adopt a face-on orientation. This kind of orientational change across the semiconductor thin film has been previously observed in semiconductor films in OFETs.[48] Here, it is most likely related to the completely different crystallization behaviors of the molecules on the hydrophobic self-assembled polymer surface versus in the bulk semiconductor film during cooling from the LC phase at 150 °C. This difference is caused by the fact that kinetic/thermodynamic parameters (e.g., surface energy, nearby electronic/structural properties, dielectric of the medium) that govern the crystallization process are totally different on the hydrophobic self-assembled polymer surface and in the bulk semiconductor film.[49] In the literature, the effect of thermal treatments of the LC phase on the charge-transport properties of the corresponding OFETs has been controversial.[50,51] To this end, our new columnar liquid crystalline semiconductor, **α,ω-2OD-TIFDMT**, is an important example of thermal annealing in the LC state causing a drastic decrease in electron mobility, which is consistent with some earlier results on similar alkyl-substituted small molecules with fused π-conjugated cores.[25]

3. Conclusions

We have designed, synthesized, and fully characterized a new highly soluble and air-stable liquid-crystalline n-channel semiconductor **α,ω-2OD-TIFDMT**, which exhibits a low LUMO

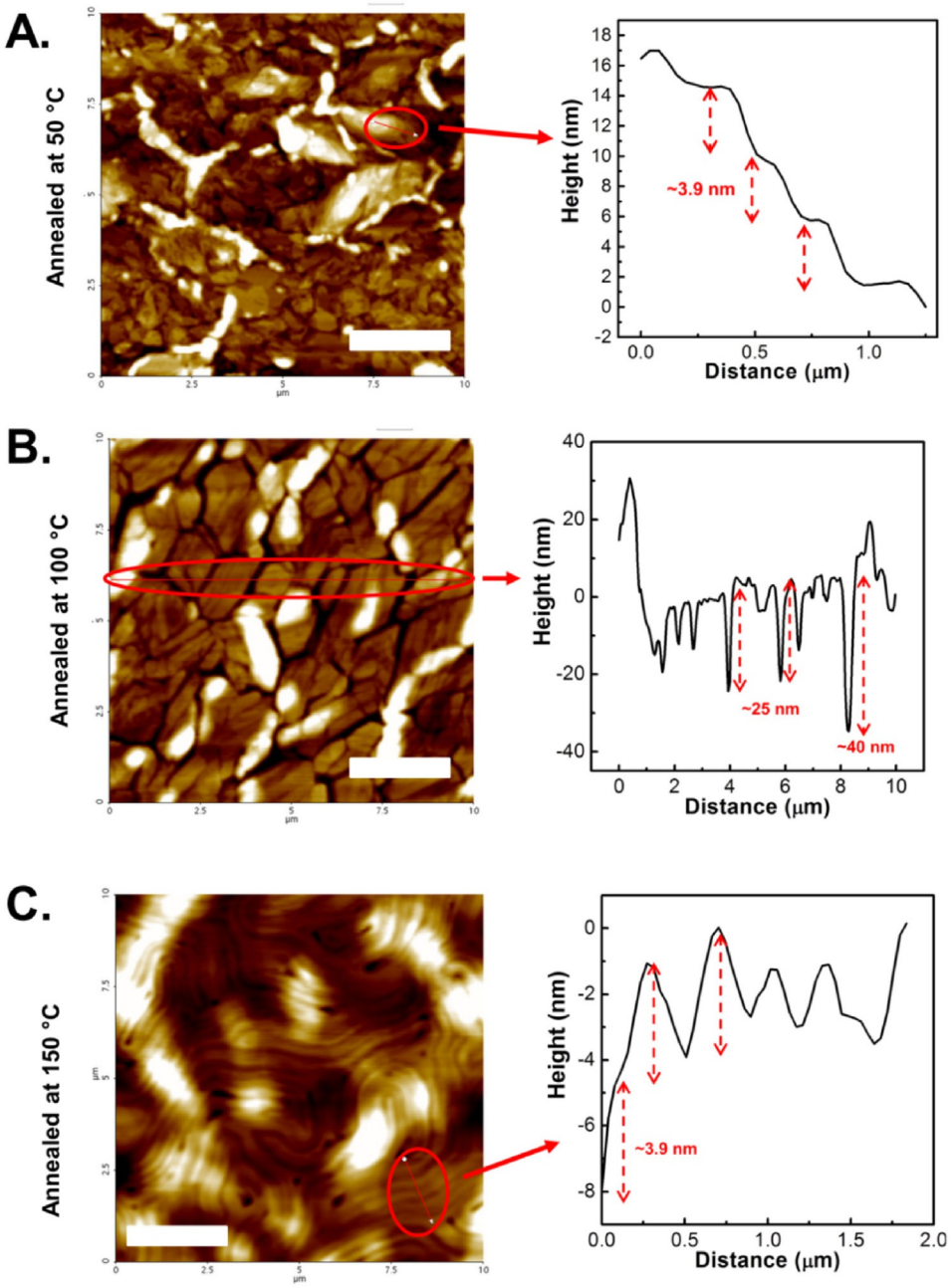

Figure 7. Step-height profiles of terraced or lamellar regions in the AFM topographic images of spin-coated **α,ω-2OD-TIFDMT** thin films annealed at A) 50, B) 100, and C) 150 °C; scale bars are 2.5 μm.

energy level of −4.19 eV and a narrow solid-state optical bandgap of 1.35 eV. DFT calculations clearly explain the electronic and geometric structure trends that occurred as a result of repositioning β-substituents to α,ω-positions. The new semiconductor exhibits excellent thermal stability (T_{onset} = 380 °C) and multiple endothermic transitions, with an isotropic transition temperature of 232 °C. The typical pseudo focal-conic fan-shaped texture of a hexagonal columnar liquid crystal phase was observed over a wide temperature range of about 139 to 232 °C. Thin films of **α,ω-2OD-TIFDMT** were prepared by using a convenient spin-coating process, and formed large (≈0.5–1.0 μm) and highly crystalline platelike grains with good interconnectivity. The microstructure consisted of mostly edge-on oriented molecules with π–π stacking interactions along the charge-transport direction. Solution-processed bottom-gate/top-contact (BG/TC) OFETs fabricated with the low-temperature-annealed (50 °C) semiconductor film demonstrated good electron mobility values of up to 0.11 $cm^2(Vs)^{-1}$ and high I_{on}/I_{off} ratios of 10^7 to 10^8 with excellent ambient stability. This indicates an enhancement of two orders of magnitude (100×) in electron mobility for low-temperature annealing in comparison to the reference β-substituted semiconductor (**β-DD-TIFDMT**). Devices stored under ambient conditions for several weeks exhibited negligible degradation in transfer characteristics and

maintained a low I_{off}, which reflected a sufficiently low LUMO energy level that stabilized electrons against the ambient redox couple (O_2/H_2O) during charge transport. Thermal annealing of the LC state gave much lower ($\approx 10^4\times$) electron mobility values, which was attributed to unfavorable changes in the semiconductor–dielectric interface during cooling from the LC phase. The current alkyl-chain engineering approach provides crucial structural guidelines for the realization of good carrier mobility at a relatively low annealing temperature for use in OFETs. We believe that the finely tuned optoelectronic and charge-transporting properties of the new semiconductor offer key advantages for use in organic photovoltaics as a non-fullerene acceptor material, and further studies are underway. Our findings prove that this new small molecule holds great promise as an air-stable and solution-processable semiconductor for the development of n-channel OFETs on low-temperature-annealed flexible plastic substrates.

Experimental Section

Materials and Methods

Reagents were purchased from Aldrich and used without further purification. All reactions were carried out under N_2 with a standard vacuum/nitrogen manifold system by using Schlenk techniques. Commercial dried solvents were used in inert-atmosphere reactions. Flash column chromatography was carried out by using 230–400 mesh silica gel from Merck. The $^1H/^{13}C$ NMR spectroscopy characterizations were performed by using a Bruker 400 spectrometer (^1H, 400 MHz; ^{13}C, 100 MHz), and elemental compositions were determined by using a Leco Truspec Micro model instrument. Thermogravimetric analysis (TGA) and differential scanning calorimetry (DSC) characterizations were performed by using Perkin–Elmer Diamond model instruments under nitrogen at a heating rate of 10 °C min^{-1}. The optical texture observation was performed by using a polarized optical microscope (Leitz Wetzlar Orthoplan-pol) equipped with a hot stage (Linkam TMS 93) and a temperature controller (Linkam LNP). Cyclic voltammetry measurements were performed by using a C3 Cell Stand equipped with an Epsilon potentiostat/galvanostat (Bioanalytical Systems, Lafayette, IN). UV/Vis absorption spectra were recorded by using a Shimadzu, UV-1800 UV/Vis spectrophotometer. MALDI-TOF spectrometry was performed by using a Bruker Microflex LT MALDI-TOF-MS instrument. The optimization of molecular geometries and the analysis of frontier molecular orbitals were carried out by using DFT at the B3LYP/6-31G** level by using Gaussian 09.[52] Scheme S1 shows the synthesis of 2,8-dibromoindeno[1,2-b]fluorene-6,12-dione (**IFDK-Br2**), 2-trimethylstannyl-5-(2-ethylhexyl)thiophene, and 2-trimethylstannyl-5-(2-octyldodecyl)thiophene, which were prepared in accordance with the reported procedures.[6]

Synthesis and Characterization

2,8-Bis(5-(2-ethylhexyl)thien-2-yl)indeno[1,2-b]fluorene-6,12-dione (1)

A mixture of 2,8-dibromoindeno[1,2-b]fluorene-6,12-dione (**IFDK-Br2**; 0.500 g, 1.136 mmol), 2-trimethylstannyl-5-(2-ethylhexyl)thiophene (0.82 g, 2.272 mmol), and $Pd(PPh_3)_2Cl_2$ (79.4 mg, 0.113 mmol) in anhydrous DMF (65 mL) was heated at 125 °C under nitrogen for 18 h. After TLC indicated the completion of the reaction, the mixture was cooled to RT and evaporated to dryness to give a dark-colored crude solid. The crude product was purified by using column chromatography on silica gel (eluent: $CHCl_3$/hexanes, 9:1) to give the final product as a dark-green solid (0.37 g, 48% yield). M.p.: 292–293 °C; ^1H NMR (400 MHz, $CDCl_3$): $\delta = 0.92$ (t, $J = 7.2$ Hz, 6H), 1.26–1.40 (m, 9H), 2.74 (d, $J = 6.4$ Hz, 2H), 6.71 (d, $J = 3.6$ Hz, 1H), 7.15 (d, $J = 3.6$ Hz, 1H), 7.40 (d, $J = 7.6$ Hz, 1H), 7.63 (m, 2H), 7.75 ppm (s, 1H); ^{13}C NMR (100 MHz, $CDCl_3$): $\delta = 10.9$, 14.2, 23.0, 25.5, 28.9, 32.4, 34.2, 41.4, 115.8, 120.9, 121.0, 123.6, 126.4, 131.4, 134.6, 136.2, 139.4, 140.2, 141.3, 145.5, 192.6 ppm; IR (KBr): 1710 cm^{-1} (C=O stretching); MS (MALDI-TOF): *m/z* calcd for $C_{44}H_{46}O_2S_2$: 670 $[M]^+$; found: 671 $[M+H]^+$; elemental analysis calcd (%) for $C_{44}H_{46}O_2S_2$: C 78.76, H 6.91; found: C 78.43, H 6.98.

2,8-Bis(5-(2-octyldodecyl)thiophen-2-yl)indeno[1,2-b]fluorene-6,12-dione (2)

A mixture of 2,8-dibromo-indeno[1,2-b]fluorene-6,12-dione (**IFDK-Br2**; 0.682 g, 1.55 mmol), 2-trimethylstannyl-5-(2-octyldodecyl)thiophene (1.80 g, 3.41 mmol), and $Pd(PPh_3)_2Cl_2$ (0.109 g, 0.155 mmol) was prepared in anhydrous DMF (75 mL), and heated at 125 °C for 1 d under a nitrogen atmosphere. The reaction mixture was then cooled to RT, and the resulting mixture was evaporated to dryness under vacuum to give a dark-colored crude solid. The crude product was purified by using silica gel column chromatography (eluent: $CHCl_3$/hexanes, 7:3 v/v) to give the final pure product as a dark-green solid (0.531 g, 34.0% yield). M.p.: 135–136 °C; ^1H NMR (400 MHz, $CDCl_3$): $\delta = 0.90$ (m, 6H), 1.28–1.31 (m, 33H), 2.74 (d, $J = 6.4$ Hz, 2H), 6.68 (d, $J = 3.2$ Hz, 1H), 7.12 (d,, $J = 3.6$ Hz 1H), 7.38 (d, $J = 7.6$ Hz, 1H), 7.60 (m, 2H), 7.70 ppm (s, 1H); ^{13}C NMR (100 MHz, $CDCl_3$): $\delta = 14.1$, 22.7, 26.6, 29.3, 29.4, 29.7, 29.8, 29.9, 30.0, 31.9, 33.2, 34.7, 40.0, 115.7, 120.8, 120.9, 123.5, 126.4, 131.3, 134.6, 136.1, 139.4, 140.2, 141.2, 145.4, 145.5, 192.5 ppm; MS (MALDI-TOF): *m/z* calcd for $C_{68}H_{94}O_2S_2$: 1008 $[M]^+$; found: 1009 $[M+H]^+$; elemental analysis calcd (%) for $C_{68}H_{94}O_2S_2$: C 81.06, H 9.40; found: C 81.31, H 9.52.

2,2′-(2,8-Bis(5-(2-ethylhexyl)thiophen-2-yl)indeno[1,2-b]fluorene-6,12-diylidene)dimalononitrile (α,ω-2EH-TIFDMT)

2,8-Bis(5-(2-ethylhexyl)thiophen-2-yl)indeno[1,2-b]fluorene-6,12-dione (**1**; 181.16 mg, 0.270 mmol) and malononitrile (0.25 g, 3.785 mmol) were dissolved in anhydrous chlorobenzene (30 mL) under nitrogen. Then, pyridine (0.41 mL, 5.09 mmol) and $TiCl_4$ (0.293 mL, 2.676 mmol) were added and the reaction mixture was heated at 110 °C for 5 h under a nitrogen atmosphere. When the resulting reaction mixture was cooled to RT for work-up, the dark-colored crude product precipitated from the reaction mixture. Due to its extremely low solubility in organic solvents, no further purification was performed on this crude material (0.135 g, 65% crude yield).

2,2′-(2,8-Bis(5-(2-octyldodecyl)thiophen-2-yl)indeno[1,2-b]fluorene-6,12-diylidene)dimalononitrile (α,ω-2OD-TIFDMT)

2,8-Bis(5-(2-octyldodecyl)thiophen-2-yl)indeno[1,2-b] fluorene-6,12-dione (**2**;0.300 g, 0.297 mmol) and malononitrile (0.275 g, 4.164 mmol) were dissolved in anhydrous chlorobenzene (35 mL) under nitrogen. Then, pyridine (0.457 mL, 5.651 mmol) and $TiCl_4$ (0.326 mL, 2.974 mmol) were added and the reaction mixture was heated at 110 °C for 5 h under a nitrogen atmosphere. The resulting reaction mixture was cooled to RT, quenched with water, and

the product was extracted with chloroform. The organic phase was washed with water, dried over Na_2SO_4, filtered, and evaporated to dryness to give the crude product as a dark-colored solid. The crude was purified by using silica gel column chromatography (eluent: chloroform), which gave the pure product as a black solid (0.237 g, 72.2% yield). M.p.: 230–231 °C; ^{1}H NMR (400 MHz, $CDCl_3$): $\delta = 0.89$ (m, 6H), 1.28 (s, 31H), 1.59 (s, 4H), 2.75 (d, $J = 8.0$ Hz, 2H), 6.73 (d, $J = 4.0$ Hz, 1H), 7.18 (d, $J = 4.0$ Hz, 1H), 7.49 (d, $J = 8.0$ Hz, 1H), 7.64 (t, $J = 8.0$ Hz, 1H), 8.29 (s, 1H), 8.42 ppm (s, 1H); ^{13}C NMR (100 MHz, $CDCl_3$): $\delta = 14.1$, 22.6, 26.5, 29.2, 29.8, 31.9, 33.0, 34.8, 39.9, 78.3, 113.0, 117.4, 121.3, 122.8, 124.0, 126.5, 131.0, 134.7, 136.7, 138.4, 139.4, 142.7, 146.5, 159.1 ppm; MS (MALDI-TOF): *m/z* calcd for $C_{74}H_{94}N_4S_2$: 1103.69 $[M]^+$; found: 1103.12 $[M]^+$; elemental analysis calcd (%) for $C_{74}H_{94}N_4S_2$: C 80.53, H 8.58, N 5.08; found: C 80.89, H 8.72, N 5.32.

Device Fabrication and Characterization

Top-contact/bottom-gate (TC/BG) OFET devices were fabricated on highly n-doped silicon wafers with a thermally oxidized SiO_2 dielectric layer (300 nm thick; capacitance per unit area (C_i) = 11.4 nF cm^{-2}). The substrates were cleaned by sonication in acetone for 10 min and then treated with oxygen plasma cleaning for 5 min (Harrick plasma, PDC-32G, 18 W). To achieve a favorable dielectric–semiconductor interface, the dielectric surface was treated with a PS-brush monolayer ($M_w = 1.7$–28 kg mol^{-1}) by following the reported procedures.[43,53,54] The organic semiconductor layer (**α,ω-2OD-TIFDMT**) was deposited by spin coating on the PS-brush-treated gate–dielectric substrates. For the spin-coating process, **α,ω-2OD-TIFDMT** was first dissolved in 1,2,4-trichlorobenzene (8 mg mL^{-1}) and the solution was spin-coated at a slow spin rate (300 rpm for 900 s) to form large crystallites.[42] The solution-processed substrates were annealed in a vacuum oven at different temperatures (50, 100, 150 °C) for 30 min. The semiconductor film thickness (40–50 nm) was measured by using a profilometer (DEKTAK-XT, Bruker). The source-drain electrodes were deposited by thermal evaporation (deposition rate = 0.2 Å s^{-1}) of Au layers (50 nm) to give various channel lengths (L; 100 and 50 μm) and widths (W; 1000 and 500 μm). The electronic performance of the OFET devices was measured under ambient conditions at RT by using a Keithley 4200-SCS semiconductor characterization system. The transistor characteristics in the saturation regime, such as charge-carrier mobility (μ) and threshold voltages (V_T), were extracted from Equation (1):

$$\mu_{sat} = (2 I_{DS} L)/[W C_i (V_G - V_T)^2] \quad (1)$$

in which I_{DS} is the drain current, L and W are the channel length and width, respectively, C_i is the areal capacitance of the gate dielectric, V_G is the gate voltage, and V_T is the threshold voltage. The surface morphology and out-of-plane crystallinity of the semiconductor thin films were characterized by using atomic force microscopy (AFM, NX10, Park systems) and X-ray diffraction (XRD, Smartlab, Rigaku).

Supplementary Data

The Supporting Information includes synthetic procedures and characterizations for compounds 2,8-dibromoindeno[1,2-b]fluorene-6,12-dione (**IFDK-Br2**), 2-trimethylstannyl-5-(2-ethylhexyl)thiophene, and 2-trimethylstannyl-5-(2-octyldodecyl)thiophene, Figures S1–S4 (^{1}H/^{13}C NMR spectra, MALDI-TOF spectrum, and ATR-FTIR spectra of **α,ω-2OD-TIFDMT**), Figure S5 (optimized molecular geometries (DFT, B3LYP/6-31G**) of **β-DD-TIFDMT** and **α,ω-2OD-TIFDMT**), Figure S6 (powder XRD spectra at 160 °C), Figure S7 (edge-on vs. face-on aligned LC phases during cooling), and Figure S8 (transfer plot of the OFET devices after ambient storage).

Acknowledgements

H.U. and R.O. acknowledge support from the AGU-BAP (Abdullah Gül University- Scientific Research Projects Funding Program) (FOA-2015-24 and FYL-2016-65). H.U. acknowledges support from the Turkish Academy of Sciences, The Young Scientists Award Program (TUBA-GEBİP 2015), and The Science Academy, Young Scientist Award Program (BAGEP 2014). C.K. acknowledges support from the Development of Space Core Program (2016M1A3A3A02016885) and from the Basic Science Research Program through the National Research Foundation of Korea (NRF-2014R1A1A1A05002158).

Conflict of Interest

The authors declare no conflict of interest.

Keywords: charge-carrier mobility · field-effect transistors · liquid crystals · semiconductors · solution processing

[1] M. Madru, G. Guillaud, M. A. Sadoun, M. Maitrot, C. Clarisse, M. L. Contellec, J.-J. André, J. Simon, *Chem. Phys. Lett.* **1987**, *142*, 103–105.
[2] R. Madru, G. Guillaud, M. Al Sadoun, M. Maitrot, J.-J. André, J. Simon, R. Even, *Chem. Phys. Lett.* **1988**, *145*, 343–346.
[3] H. E. Katz, Z. Bao, S. L. Gilat, *Acc. Chem. Res.* **2001**, *34*, 359–369.
[4] L. Zhang, A. Fonari, Y. Liu, A.-L. M. Hoyt, H. Lee, D. Granger, S. Parkin, T. P. Russell, J. E. Anthony, J.-L. Brédas, V. Coropceanu, A. L. Briseno, *J. Am. Chem. Soc.* **2014**, *136*, 9248–9251.
[5] M. Ozdemir, D. Choi, G. Kwon, Y. Zorlu, B. Cosut, H. Kim, A. Facchetti, C. Kim, H. Usta, *ACS Appl. Mater. Interfaces* **2016**, *8*, 14077–14087.
[6] M. Ozdemir, D. Choi, G. Kwon, Y. Zorlu, H. Kim, M.-G. Kim, S. Seo, U. Sen, M. Citir, C. Kim, H. Usta, *RSC Adv.* **2016**, *6*, 212–226.
[7] C. Wang, Y. Qin, Y. Sun, Y. S. Guan, W. Xu, D. Zhu, *ACS Appl. Mater. Interfaces* **2015**, *7*, 15978–15987.
[8] V. Figà, C. Chiappara, F. Ferrante, M. P. Casaletto, F. Principato, S. Cataldo, Z. Chen, H. Usta, A. Facchetti, B. Pignataro, *J. Mater. Chem. C* **2015**, *3*, 5985–5994.
[9] U. Sen, H. Usta, O. Acar, M. Citir, A. Canlier, A. Bozkurt, A. Ata, *Macromol. Chem. Phys.* **2015**, *216*, 106–112.
[10] R. P. Ortiz, H. Herrera, C. Seoane, J. L. Segura, A. Facchetti, T. J. Marks, *Chem. Eur. J.* **2012**, *18*, 532–543.
[11] W. W. H. Wong, T. Birendra Singh, D. Vak, W. Pisula, C. Yan, X. Feng, E. L. Williams, K. L. Chan, Q. Mao, D. J. Jones, M. Chang-Qi, K. Müllen, P. Bäuerle, A. B. Holmes, *Adv. Funct. Mater.* **2010**, *20*, 927–928.
[12] L. Duan, L. Hou, T.-W. Lee, J. Qiao, D. Zhang, G. Dong, L. Wang, Y. Qiu, *J. Mater. Chem.* **2010**, *20*, 6392.
[13] H. Usta, W. C. Sheets, M. Denti, G. Generali, R. Capelli, S. Lu, X. Yu, M. Muccini, A. Facchetti, *Chem. Mater.* **2014**, *26*, 6542–6556.
[14] J. K. Borchardt, *Mater. Today* **2004**, *7*, 42–46.
[15] S. Fabiano, H. Usta, R. Forchheimer, X. Crispin, A. Facchetti, M. Berggren, *Adv. Mater.* **2014**, *26*, 7438–7443.
[16] H. Usta, A. Facchetti, T. J. Marks, *Acc. Chem. Res.* **2011**, *44*, 501–510.
[17] S. S. Cheng, P. Y. Huang, M. Ramesh, H. C. Chang, L. M. Chen, C. M. Yeh, C. L. Fung, M. C. Wu, C. C. Liu, C. Kim, H.-C. Lin, M.-C. Chen, C.-W. Chu, *Adv. Funct. Mater.* **2014**, *24*, 2057–2063.

[18] M. Mamada, H. Shima, Y. Yoneda, T. Shimano, N. Yamada, K. Kakita, T. Machida, Y. Tanaka, S. Aotsuka, D. Kumaki, S. Tokito, *Chem. Mater.* **2015**, *27*, 141 – 147.
[19] C. B. Nielsen, S. Holliday, H.-Y. Chen, S. J. Cryer, I. McCulloch, *Acc. Chem. Res.* **2015**, *48*, 2803 – 2812.
[20] P. Kumaresan, S. Vegiraju, Y. Ezhumalai, S. Yau, C. Kim, W.-H. Lee, M.-C. Chen, *Polymers (Basel, Switz.)* **2014**, *6*, 2645 – 2669.
[21] N. Azum, L. A. Taib, Y. M. Al Angari, A. M. Asiri, M. Denti, W. Zhao, H. Usta, A. Facchetti, *Thin Solid Films* **2016**, *616*, 320 – 327.
[22] M.-C. Chen, S. Vegiraju, C.-M. Huang, P.-Y. Huang, K. Prabakaran, S. L. Yau, W.-C. Chen, W.-T. Peng, I. Chao, C. Kim, Y.-T. Tao, *J. Mater. Chem. C* **2014**, *2*, 8892 – 8902.
[23] A. Facchetti, M.-H. Yoon, C. L. Stern, H. E. Katz, T. J. Marks, *Angew. Chem. Int. Ed.* **2003**, *42*, 3900 – 3903; *Angew. Chem.* **2003**, *115*, 4030 – 4033.
[24] H. Usta, A. Facchetti, T. J. Marks, *J. Am. Chem. Soc.* **2008**, *130*, 8580 – 8581.
[25] W.-L. Liau, T.-H. Lee, J.-T. Chen, C.-S. Hsu, *J. Mater. Chem. C* **2016**, *4*, 2284 – 2288.
[26] B. N. Veerabhadraswamy, H. K. Dambal, D. S. S. Rao, C. V. Yelamaggad, *ChemPhysChem* **2016**, *17*, 2225 – 2237.
[27] Z. Zhao, Z. Wang, Y. Hu, X. Yang, H. Li, X. Gao, D. Zhu, *J. Org. Chem.* **2013**, *78*, 12214 – 12219.
[28] B. R. Kaafarani, *Chem. Mater.* **2011**, *23*, 378 – 396.
[29] M. Funahashi, A. Sonoda, *Phys. Chem. Chem. Phys.* **2014**, *16*, 7754 – 7763.
[30] H. Iino, T. Usui, J.-I. Hanna, *Nat. Commun.* **2015**, *6*, 6828.
[31] Y. Takaki, R. Ozawa, T. Kajitani, T. Fukushima, M. Mitsui, K. Kobayashi, *Chem. Eur. J.* **2016**, *22*, 16760 – 16764.
[32] H. Usta, C. Risko, Z. Wang, H. Huang, M. K. Deliomeroglu, A. Zhukhovitskiy, A. Facchetti, T. J. Marks, *J. Am. Chem. Soc.* **2009**, *131*, 5586 – 5608.
[33] D. S. Rampon, F. S. Rodembusch, J. M. F. M. Schneider, I. H. Bechtold, P. F. B. Gonçalves, A. A. Merlo, P. H. Schneider, *J. Mater. Chem.* **2010**, *20*, 715 – 722.
[34] K. Sun, Z. Xiao, S. Lu, W. Zajaczkowski, W. Pisula, E. Hanssen, J. M. White, R. M. Williamson, J. Subbiah, J. Ouyang, A. B. Holmes, W. W. H. Wong, D. J. Jones, *Nat. Commun.* **2015**, *6*, 6013.
[35] S.-J. Yoon, J. H. Kim, K. S. Kim, J. W. Chung, B. Heinrich, F. Mathevet, P. Kim, B. Donnio, A.-J. Attias, D. Kim, S. Y. Park, *Adv. Funct. Mater.* **2012**, *22*, 61 – 69.
[36] H. L. Ni, H. Monobe, P. Hu, B. Q. Wang, Y. Shimizu, K. Q. Zhao, *Liq. Cryst.* **2013**, *40*, 411 – 420.
[37] S. Laschat, A. Baro, N. Steinke, F. Giesselmann, C. Hägele, G. Scalia, R. Judele, E. Kapatsina, S. Sauer, A. Schreivogel, M. Tosoni, *Angew. Chem. Int. Ed.* **2007**, *46*, 4832 – 4887; *Angew. Chem.* **2007**, *119*, 4916 – 4973.
[38] R. K. Gupta, S. K. Pathak, B. Pradhan, D. S. Shankar Rao, S. Krishna Prasad, A. S. Achalkumar, *Soft Matter* **2015**, *11*, 3629 – 3636.
[39] L. Oldridge, M. Kastler, K. Müllen, *Chem. Commun.* **2006**, 885 – 887.
[40] A. Riaño, P. Mayorga Burrezo, M. J. Mancheño, A. Timalsina, J. Smith, A. Facchetti, T. J. Marks, J. T. López Navarrete, J. L. Segura, J. Casado, R. P. Ortiz, *J. Mater. Chem. C* **2014**, *2*, 6376 – 6386.
[41] L. Zhang, N. S. Colella, B. P. Cherniawski, S. C. B. Mannsfeld, A. L. Briseno, *ACS Appl. Mater. Interfaces* **2014**, *6*, 5327 – 5343.
[42] K. Wei Chou, H. Ullah Khan, M. R. Niazi, B. Yan, R. Li, M. M. Payne, J. E. Anthony, D.-M. Smilgies, A. Amassian, *J. Mater. Chem. C* **2014**, *2*, 5681.
[43] S. H. Park, H. S. Lee, J.-D. Kim, D. W. Breiby, E. Kim, Y. D. Park, D. Y. Ryu, D. R. Lee, J. H. Cho, *J. Mater. Chem.* **2011**, *21*, 15580.
[44] H. Usta, C. Newman, Z. Chen, A. Facchetti, *Adv. Mater.* **2012**, *24*, 3678 – 3684.
[45] D. M. de Leeuw, M. M. J. Simenon, A. R. Brown, R. E. F. Einerhand, *Synth. Met.* **1997**, *87*, 53 – 59.
[46] B. A. Jones, A. Facchetti, M. R. Wasielewski, T. J. Marks, *J. Am. Chem. Soc.* **2007**, *129*, 15259 – 15278.
[47] H. Zhang, X. Guo, J. Hui, S. Hu, W. Xu, D. Zhu, *Nano Lett.* **2011**, *11*, 4939 – 4946.
[48] G. Kim, S.-J. Kang, G. K. Dutta, Y.-K. Han, T. J. Shin, Y.-Y. Noh, C. Yang, *J. Am. Chem. Soc.* **2014**, *136*, 9477 – 9483.
[49] D. E. Martínez-Tong, C. Ruzié, Y. H. Geerts, M. Sferrazza, *ChemPhysChem* **2016**, *17*, 1174 – 1179.
[50] I. McCulloch, M. Heeney, C. Bailey, K. Genevicius, I. MacDonald, M. Shkunov, D. Sparrowe, S. Tierney, R. Wagner, W. Zhang, M. L. Chabinyc, R. J. Kline, M. D. McGehee, M. F. Toney, *Nat. Mater.* **2006**, *5*, 328 – 333.
[51] S. Sergeyev, W. Pisula, Y. H. Geerts, *Chem. Soc. Rev.* **2007**, *36*, 1902.
[52] Gaussian 09, Revision C.01, M. J. Frisch, G. W. Trucks, H. B. Schlegel, G. E. Scuseria, M. A. Robb, J. R. Cheeseman, G. Scalmani, V. Barone, B. Mennucci, G. A. Petersson, H. Nakatsuji, M. Caricato, X. Li, H. P. Hratchian, A. F. Izmaylov, J. Bloino, G. Zheng, J. L. Sonnenberg, M. Hada, M. Ehara, K. Toyota, R. Fukuda, J. Hasegawa, M. Ishida, T. Nakajima, Y. Honda, O. Kitao, H. Nakai, T. Vreven, J. A. Montgomery, Jr., J. E. Peralta, F. Ogliaro, M. Bearpark, J. J. Heyd, E. Brothers, K. N. Kudin, V. N. Staroverov, T. Keith, R. Kobayashi, J. Normand, K. Raghavachari, A. Rendell, J. C. Burant, S. S. Iyengar, J. Tomasi, M. Cossi, N. Rega, J. M. Millam, M. Klene, J. E. Knox, J. B. Cross, V. Bakken, C. Adamo, J. Jaramillo, R. Gomperts, R. E. Stratmann, O. Yazyev, A. J. Austin, R. Cammi, C. Pomelli, J. W. Ochterski, R. L. Martin, K. Morokuma, V. G. Zakrzewski, G. A. Voth, P. Salvador, J. J. Dannenberg, S. Dapprich, A. D. Daniels, O. Farkas, J. B. Foresman, J. V. Ortiz, J. Cioslowski, and D. J. Fox, Gaussian, Inc., Wallingford CT, **2010**.
[53] C. Kim, A. Facchetti, T. J. Marks, *Adv. Mater.* **2007**, *19*, 2561 – 2566.
[54] B. Kim, D. Y. Ryu, V. Pryamitsyn, V. Ganesan, *Macromolecules* **2009**, *42*, 7919 – 7923.

Manuscript received: December 27, 2016
Accepted Article published: January 17, 2017
Final Article published: February 22, 2017